Ph.D. Dissertation of Medicine

Algorithm development for detecting the putaminal lateral rim in 3T susceptibility-weighted imaging and quantitative approach to the differential diagnosis of multiple system atrophy with predominant parkinsonism

3T 자화강조영상의 조가비핵 가장자리 감지를 위한 알고리즘 개발 및 파킨슨형다계통위축증의 감별진단을 위한 정량적 접근

August 2022

Graduate School of Medicine
Seoul National University
Translational Medicine Major

Woong-Woo Lee

Algorithm development for detecting the putaminal lateral rim in 3T susceptibility-weighted imaging and quantitative approach to the differential diagnosis of multiple system atrophy with predominant parkinsonism

Beomseok Jeon

Submitting a Ph.D. Dissertation of
Medicine

April 2022

Graduate School of Medicine
Seoul National University
Translational Medicine Major

Woong-Woo Lee

Confirming the Ph.D. Dissertation written by
Woong-Woo Lee
July 2022

Chair	Kwang Suk Park	(Seal)
Vice Chair	Beomseok Jeon	(Seal)
Examiner	Ki-Young Jung	(Seal)
Examiner	Chul-Ho Sohn	(Seal)
Examiner	Byung-Kun Kim	(Seal)

Abstract

Background and Objectives: Putaminal iron deposition is an important feature that helps differentiate multiple system atrophy with parkinsonism (MSA-p) from Parkinson's disease (PD). Most previous studies used visual assessment for brain MRI or quantitative methods with manual manipulation to perform this differentiation. In addition, they did not consider differences in fundamental iron distribution by age, location, and individual characteristics. Early detection is also a crucial goal in an imaging-based diagnosis. We developed a new semiautomated diagnostic algorithm using 3T-MR susceptibility-weighted imaging (SWI) and investigated its diagnostic value for early MSA-p to overcome rater-dependent inconsistency and normalization issues and improve diagnostic performance.

Methods: This study included 26 MSA-p, 68 PD, and 41 normal control (NC) subjects. The algorithm was developed in 2 steps: 1) determine the image containing the remarkable putaminal margin and 2) calculate the phase-shift values (PSVs), which reflect the iron concentration along the lateral margin. There were two approaches: a segment-based approach and a continuous curve-based approach. In the segment-based approach, we divided the entire lateral rim into 10 subparts and used the mean value of each subpart. The continuous curve-based approach used all PSVs of

each subject, not the region of interest. The next step was to identify the best differentiating conditions among several combinations. The various representative PSVs of each subject were examined to figure out the most effective diagnostic set.

Results: The algorithm detected the putaminal lateral rims of all MSA-p, while it did not discriminate those of 8 PD and 2 NC subjects. The scatterplot shows that the raw PSVs were present along the lateral margin of the putamen in each group. It demonstrates an anterior-to-posterior gradient that was identified most frequently in MSA-p, while the most anterior parts had consistent patterns and similar PSVs (p=0.517) regardless of disease group. In the segment-based approach, age was correlated with PSV in all segments except for Segment 10. The PSV of Segment 1 showed a better linear correlation with all the segments than age. The regression equations with age and the PSV of Segment 1 were utilized for estimating the normalized PSVs. The highest area under the receiver operating characteristic curve (AUC) was 0.872 for separating MSA-p from PD. In the continuous curve-based approach, the average PSVs of 5 anterior points were used for normalization. The AUC of MSA-p versus PD was 0.872 to 0.878 under the combination of 3 or 4 vertical pixels and one dominant side when the normalization methods were applied (80.8% sensitivity and 86.7% specificity). The AUC to differentiate MSA-p from NC was 0.883 (73.1% sensitivity and 97.4% specificity). The

subanalysis for the MSA-p patients with a longer disease duration showed better performance.

Conclusions: This semiautomated algorithm detected the lateral margin of the putamen well and provided insight into the iron distribution of the putaminal rim of MSA-p. With a new personalized approach to reflect the individual iron background, the algorithm demonstrated good performance in differentiating MSA-p from PD and NC.

Keywords: susceptibility-weighted image, semiautomation, multiple system atrophy, Parkinson's disease, putamen

Student Number: 2013-31163

Table of Contents

Figures and Tables

Figures

Tables

Chapter 1. Introduction

1.1. Study Background

Multiple system atrophy (MSA) is a rapidly progressive neurodegenerative disease characterized by parkinsonism, cerebellar dysfunction, and dysautonomia.[1, 2] The key findings of MSA neuropathology are widespread α-synuclein-positive glial cytoplasmic inclusions and neurodegeneration in the striatonigral or olivopontocerebellar system.[3, 4] These pathological features became the essential condition for "definite MSA" or "neuropathologically established MSA" in the consensus criteria for the diagnosis of MSA.[2, 5] However, it is not feasible to make a pathological diagnosis of living patients.

The diagnostic criteria of probable MSA and possible MSA in the second consensus criteria are based on clinical features of automatic dysfunction, parkinsonism, and cerebellar dysfunction.[2] However, there are several difficulties associated with providing an early differential diagnosis with these clinical criteria. Autonomic dysfunctions, a core feature of MSA, were not observed at onset in 59% of patients, although they developed in most cases throughout

the disease period.[6] In addition, many cases of MSA with predominant parkinsonism (MSA-p) show asymmetric onset (43%) and L-dopa responsiveness (42.5%).[7, 8] Thus, early MSA-p can mimic Parkinson's disease (PD).[9, 10] This clinical heterogeneity contributes to the low level of diagnostic accuracy.[11, 12] The new MSA diagnostic criteria reflected these limitations and made "clinically probable MSA", where autonomic dysfunction and L-dopa responsiveness are not essential.[5]

Since Bhattacharya et al. suggested a diagnostic algorithm for MSA, brain magnetic resonance imaging (MRI) has received attention as a promising tool for differential diagnoses.[13] The representative findings of conventional MRI for MSA are reported as follows: (1) atrophy, low signal intensity on T2, and lateral hyperintensity rim sign on T2 for the putamen; (2) atrophy and a "hot-cross bun" sign for the pons; and (3) atrophy and high signal intensity of the middle cerebellar peduncle on T2 for the cerebellum. As MRI and nuclear imaging data became more available for MSA, diagnostic imaging findings were newly introduced in the second set of consensus criteria for additional features: (1) atrophy on MRI of the putamen, middle cerebellar peduncle, pons, or cerebellum; and (2) hypometabolism on FDG-PET in the putamen, brainstem, or cerebellum in possible MSA-p.[2] Recent advances in the instruments

themselves and processing techniques have contributed to increased diagnostic accuracy.[14, 15]

While MSA-specific MRI findings were not essential in the second consensus criteria, the revised MSA diagnostic criteria requires at least one MRI marker to diagnose a "clinically established MSA."[2, 5] In particular, iron-sensitive sequences were approved as an MRI marker when confirming putaminal changes. This means how important putaminal iron deposition is in the diagnosis of MSA. Abundant accumulations of iron and putaminal atrophy in MSA-p, although it is unclear which feature appears first, are commonly found in posterolateral areas of the putamen.[16-18]

The early version of iron-sensitive imaging techniques is T2*-weighted magnitude imaging (T2*WI).[19, 20] Susceptibility-weighted imaging (SWI) is the combination of magnitude and phase maps, so its sensitivity and spatial resolution are quite better than T2*WI. Quantitative susceptibility mapping (QSM) is a more advanced technique that makes each voxel contain a calculated quantitative value of iron. SWI is more widely utilized because QSM needs more time to be undertaken. These iron-sensitive imaging techniques have been developed to achieve an early and accurate diagnosis of MSA-p.[19, 21, 22]

Although the advanced MR processing techniques improved the sensitivity and specificity for diagnosing MSA-p,[23] there are still unsolved issues related to obtaining a higher diagnostic yield. The critical issues are rater-related factors. The selected image cut and region of interest may be inconsistent between raters. Thus, many studies have suggested analyzing interrater reliability. In addition, the issue of intrarater reliability should be considered, especially in the case of visual assessment. Quantification has been presented as an alternative method of overcoming the issue of inconsistency related to a visual assessment.[22] However, although the quantified analysis differentiated MSA-p from PD relatively well, it seems to still be arbitrary in determining the region of interest.

Individualization is another important issue. Iron distribution patterns in the normal putamen change depending on age and location.[24] Older age and a more posterolateral location in the putamen are more likely to result in a higher iron concentration. In other words, the iron distribution of the putamen in aged individuals can appear like that in MSA-p patients. Therefore, regardless of the consideration of the individual iron distribution pattern, the fixed cut-off value may not be suitable for the image-based differentiation of MSA-p from the normal population or PD patients.

For imaging to be beneficial, it is crucial that research be conducted at an early stage when the clinical diagnosis is unclear, not after the disease has progressed significantly. This study targeted MSA-p patients who underwent MRI at an early stage.

1.2. Purpose of Research

The current study aimed to overcome the inconsistency and individualization issues and to enhance the diagnostic accuracy for MSA-p in an early phase of the disease with 3T-MR SWI. We developed a semiautomated algorithm to detect the later rim well and tried to find an appropriate normalization method to overcome the variations by age and individual unique iron backgrounds.

Chapter 2. Methods

2.1. Subjects

The included patients fulfilled the following criteria: 1) visited the Movement Disorder Center of the Seoul National University Hospital due to parkinsonism, 2) underwent 3T brain MRI including SWI, and 3) were clinically diagnosed with either PD or MSA-p (possible or probable MSA based on the second consensus criteria) at their last visit during the follow-up period.[2, 25] Even though some patients with MSA-p had cerebellar symptoms, all of them showed parkinsonism as an initial and/or predominant symptom. Forty-one normal control (NC) subjects who had no clinical features of neurodegenerative disorders and underwent brain MRI with the same protocol as that used in the PD and MSA-p groups were also included. Subjects who had white matter changes over Fazekas' grade 1, space-occupying or destructive lesions on brain images, or a history of neurosurgical procedures, including deep brain stimulation before brain imaging, were excluded from the study. Finally, 135 subjects (26 with MSA-p, 68 with PD, and 41 NCs) were included. Among the 26 cases with MSA-p, 20 were

diagnosed with probable MSA-p and 6 with possible MSA-p based on the final diagnosis at the last visit. Other clinical features, such as age at onset, sex, age at the brain MRI visit, and age at the last visit, were obtained from the medical records.

This study was conducted according to the Declaration of Helsinki. The study was performed retrospectively, and the records of the patients were anonymized and deidentified prior to the analysis. Written informed consent for the clinical records was waived because of the guaranteed anonymity and deidentification. The study protocol was approved by the Institutional Review Board of Seoul National University Hospital.

2.2. MRI protocol

The subjects underwent 3T brain MRI for SWI with a 32-channel head coil. Magnetom Verio (Siemens, Erlangen, Germany) was used for 3T SWI. All images that were used for the analysis were obtained along the transverse plane parallel to the anterior/posterior commissure lines. The detailed parameters were as follows: for 3T SWI, section thickness = 2 mm, TR/TE =

28.0/20.0 ms, field of view = 178 × 220 mm, matrix = 364 × 448, and number of excitations = 1. Magnitude and phase images were generated for the last SWI on the MR imaging console workstation (syngo MR B17; Siemens, Erlangen, Germany). The corrected phase images were used for the analysis according to the algorithm.

2.3. Algorithm to identify the proper target and obtain data

The shapes of the putamen vary from person to person. Thus, we developed an algorithm that consists of Part I and Part II (Figure 1). Part I identifies the axial image that has the most remarkable lateral rim of the putamen. Part II includes the algorithm to detect the margin of both putamina from the selected axial image in Part I, as well as to obtain the calculated phase-shift value (PSV) data of each point in the margin. The "height" in the algorithm indicates the number of included pixels used to calculate the average value of each point in each axial image. If '3' is input into the "height" box, the algorithm recognizes an average value of 3 sequential

pixels in the anterior-to-posterior direction as a newly calculated value of the first point (Figure 2).

In Part I, any axial image containing both putamina is selected arbitrarily to start the algorithm. Then, the algorithm automatically moves up and down to search for the appropriate axial image with the most remarkable lateral margin (using edge detection and region-growing methods). If the identified image is rotated, the proper data on the lateral rim may not be obtained. Therefore, as the first step of Part II, the algorithm rerotated the identified image based on the axis of the falx cerebri. Then, the investigator drew a crude box including the area of interest and marked the first and last points of the lateral rim for each putamen (4 points for each subject) on the selected area. Finally, the algorithm visualized the selected lateral margins of both putamina and obtained the raw data of the calculated PSVs at each location. All the above-described steps were performed repeatedly according to the "height" number, which ranged from 1 to 4. One researcher who was blinded to the diagnosis performed all the manual processes.

Figure 1. Detailed process of the algorithm

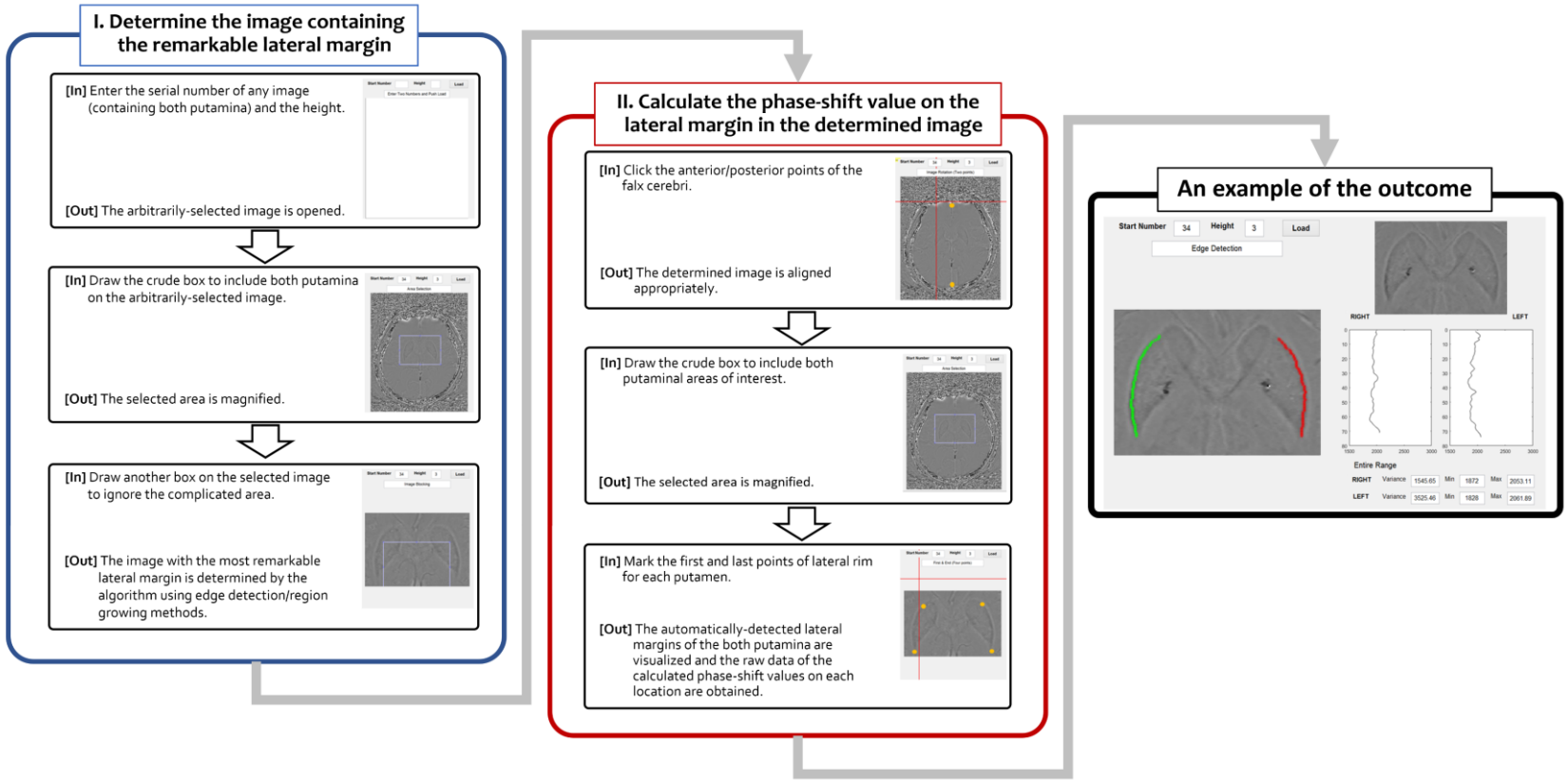

Dark and white signals indicate high and low phase-shift values, respectively.

Figure 2. Definition of the height

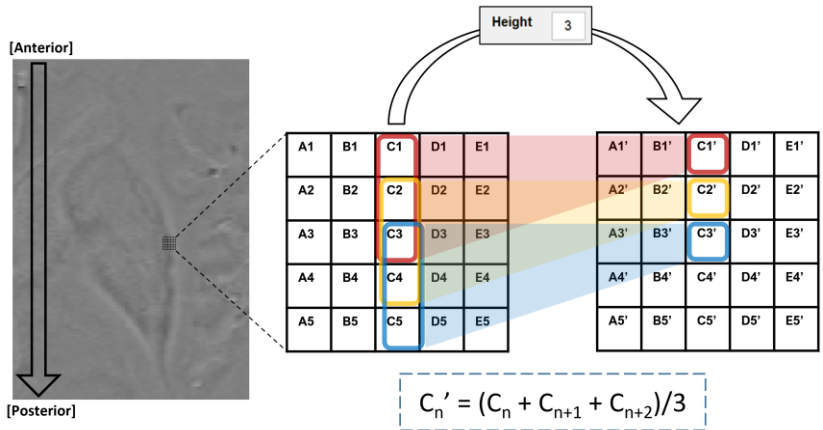

2.4. Statistics

All processes were performed using MATLAB R2015a (MathWorks, Natick, MA, USA) for algorithm development and activation. SPSS software version 21.0 (IBM Co., Armonk, NY, USA) was used for the statistical analysis. Independent t-tests and ANOVA were performed to assess the differences between the groups as appropriate. We performed a linear correlation analysis to examine the relationship between age and PSV of each segment. A multiple regression model was applied to predict normalized PSVs of each corresponding region. The receiver operating characteristic (ROC) curve was analyzed to obtain the most effective combination for the proper diagnosis of MSA-p. The statistical significance level was set at $p < 0.05$.

Chapter 3. Results

3.1. Clinical characteristics

The clinical characteristics of each group are summarized in Table 1. There were no significant differences with respect to sex and age at onset or at the time of brain MRI. The duration from onset to the time of workup was significantly shorter in the MSA-p group. The period between onset and the last visit was also shorter for MSA-p patients. Six patients (23.1%) had cerebellar symptoms, and 7 patients (26.9%) exhibited partial levodopa responsiveness in the MSA-p group.

Table 1. Clinical characteristics of each group

	MSA-p	PD	NC	*p value*
Number of subjects [male:female]	26 [11:15]	68 [35:33]	41 [16:25]	0.414
Age at brain MRI (years)	64.4 ± 10.0	64.0 ± 8.2	61.0 ± 10.3	0.189
Age at onset (years)	61.9 ± 10.6	58.2 ± 10.2	NA	0.124
Duration between onset and brain imaging (years)	2.5 ± 1.4	5.9 ± 4.9	NA	<0.001***
Duration between onset and last visit (years)	3.9 ± 1.5	8.2 ± 5.1	NA	<0.001***

MSA-p: multiple system atrophy with predominant parkinsonism, PD: Parkinson's disease, NC: normal control, NA: not applicable
***p<0.001

3.2. Application of the semiautomated quantitative algorithm

The putaminal lateral margins of all subjects in the MSA-p group were well detected, while those of 8 (11.8%) in the PD group and 2 (4.9%) in the NC group were not discriminated by the algorithm. The possible reasons for the lack of discrimination are as follows: unclear lateral margin for 2 PD patients and vascular lesions with or without diffuse homogenous signal change of the putamen for 6 PD patients and 2 NC subjects.

One hundred twenty-five (92.6%) of the 135 subjects showed well-demarcated margins (52 margins of 26 MSA-p patients, 120 margins of 60 PD patients, and 78 margins of 39 NC subjects). We scattered the raw data of each subject in each group (Figure 3). The MSA-p group showed a wide distribution of calculated PSVs intra-individually as well as inter-individually. In contrast, the PD and NC groups consistently exhibited similar values along the anterior-to-posterior direction. The most anterior parts seemed to display similar values regardless of group.

Figure 3. Scatterplot for the phase-shift values of the MSA-p, PD, and NC groups

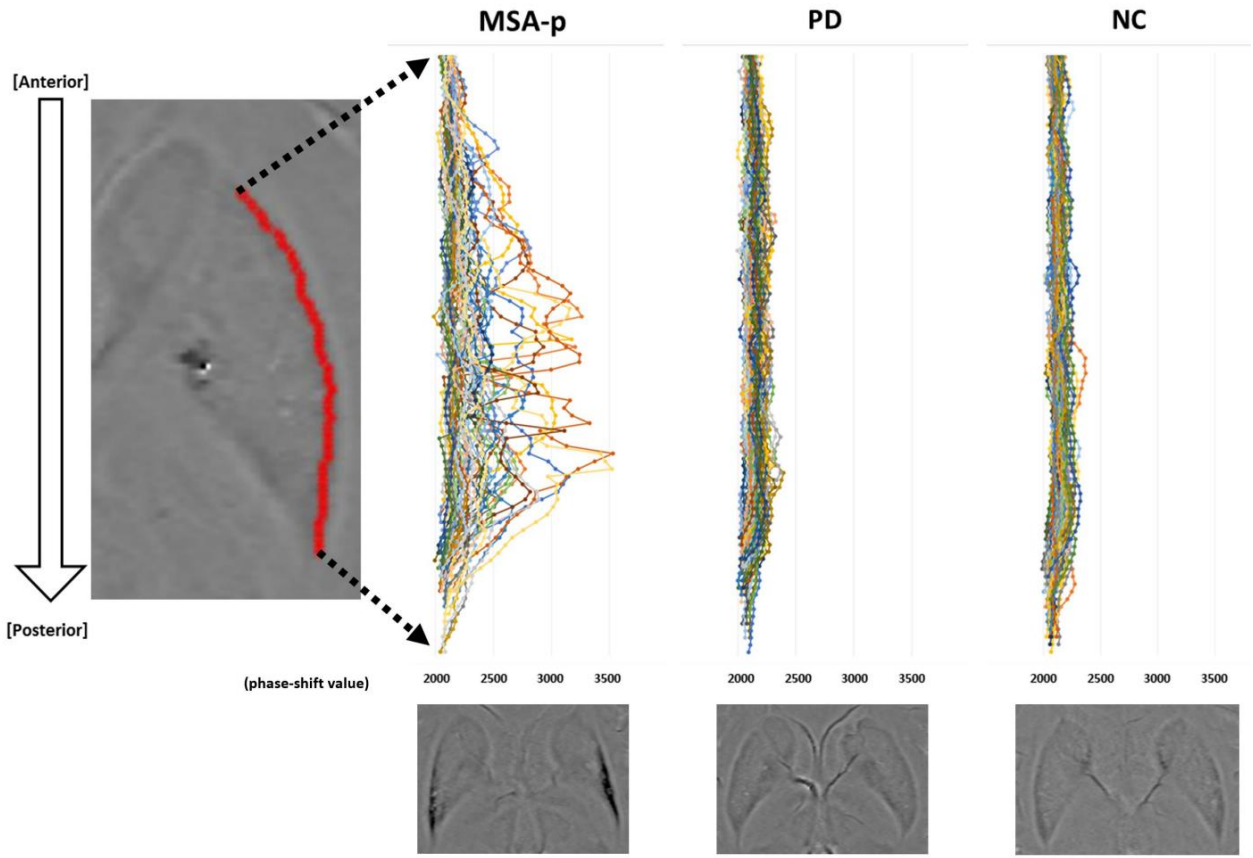

MSA-p: multiple system atrophy with predominant parkinsonism, PD: Parkinson's disease, NC: normal control
The figures below show representative examples of each group. Dark and white signals indicate high and low phase-shift values, respectively.

3.3. Segment-based approach for the lateral rim

We divided each margin into ten subparts with the same length (Figure 4). This section sets each segment's mean PSV (height=1) as its representative value.

Figure 4. Example of dividing segments

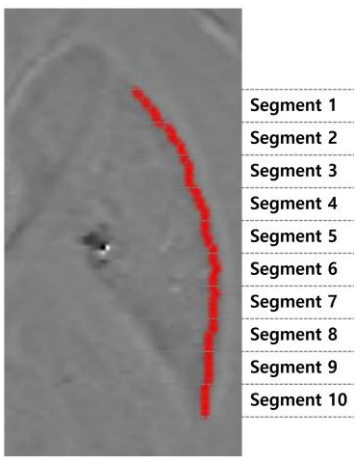

3.3.1. Segment-based comparison between groups

Figure 5 explains which location is most predominant for the highest PSV according to groups. Although all groups had Segment 9 as the most remarkable area for iron deposition, the MSA-p group had a relatively wide area (Segment 7, 8, and 9) of the maximum signal.

Figure 5. Location with maximum phase-shift value by group

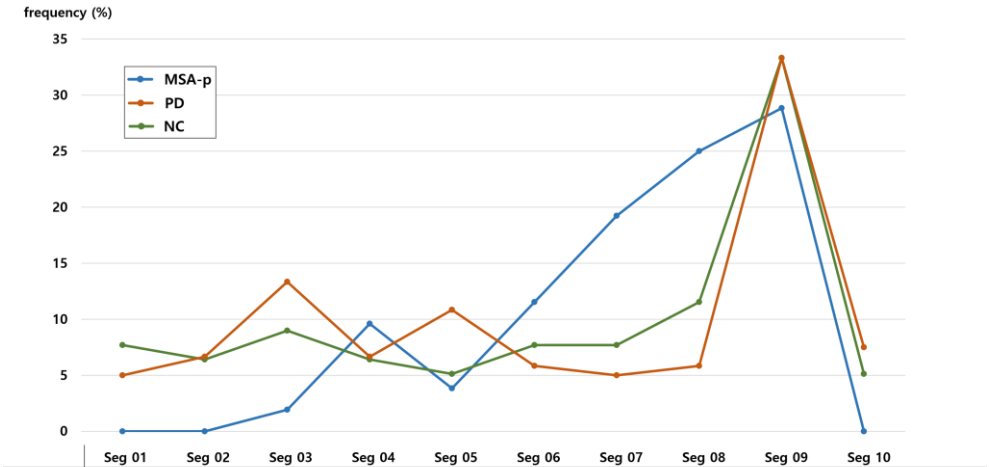

	Seg 01	Seg 02	Seg 03	Seg 04	Seg 05	Seg 06	Seg 07	Seg 08	Seg 09	Seg 10	
MSA-p	0 (0%)	0 (0%)	1 (1.9%)	5 (9.6%)	2 (3.8%)	6 (11.5%)	10 (19.2%)	13 (25%)	15 (28.8%)	0 (0%)	52 (100%)
PD	6 (5.0%)	8 (6.7%)	16 (13.3%)	8 (6.7%)	13 (10.8%)	7 (5.8%)	6 (5.0%)	7 (5.8%)	40 (33.3%)	9 (7.5%)	120 (100%)
NCI	6 (7.7%)	5 (6.4%)	7 (9.0%)	5 (6.4%)	4 (5.1%)	6 (7.7%)	6 (7.7%)	9 (11.5%)	26 (33.3%)	4 (5.1%)	78 (100%)

Seg: segment, MSA-p: multiple system atrophy with predominant parkinsonism, PD: Parkinson's disease, NC: normal control

Table 2 shows the results of segment-based comparison for PSVs between groups. Except for Segment 1, all segments revealed significant differences between groups. The MSA-p group demonstrated higher PSVs than the PD group (from Segment 2 to Segment 9) and the NC group (from Segment 2 to Segment 10). There were no statistically remarkable differences between the PD and NC groups.

Table 2. Comparison of phase-shift values between groups

	Seg 01	Seg 02	Seg 03	Seg 04	Seg 05	Seg 06	Seg 07	Seg 08	Seg 09	Seg 10
Between Groups	0.540	0.001**	<0.001***	<0.001***	<0.001***	<0.001***	<0.001***	<0.001***	<0.001***	0.005**
MSA-p vs. PD	NA	0.018*	<0.001***	<0.001***	<0.001***	<0.001***	<0.001***	<0.001***	<0.001***	0.090
MSA-p vs. NC	NA	0.001**	<0.001***	<0.001***	<0.001***	<0.001***	<0.001***	<0.001***	<0.001***	0.006**
PD vs. NC	NA	0.152	0.543	0.574	0.862	0.094	0.513	0.939	1.000	0.157

Seg: segment, MSA-p: multiple system atrophy with predominant parkinsonism, PD: Parkinson's disease, NC: normal control, vs.: versus, NA: not applicable
*p<0.05, **p<0.01, ***p<0.001

3.3.2. Anterior-to-posterior iron distribution with aging

As shown in Table 2, the PD and NC groups are not different regarding iron distribution patterns. Therefore, we analyzed the PSVs of both groups together to assess whether aging affects iron distributions in non-MSA-p subjects.

Figure 6 demonstrates PSVs of all segments according to age groups. All segments except Segment 1 and Segment 10 showed significant intergroup differences. Aging seemed to influence the increase of iron deposition in most segments, although all subgroup comparisons were not statistically significant. In this sense, age could be a confounding factor disturbing the proper diagnosis of MSA-p.

Figure 6. Age-dependent phase-shift values in non-MSA-p subjects

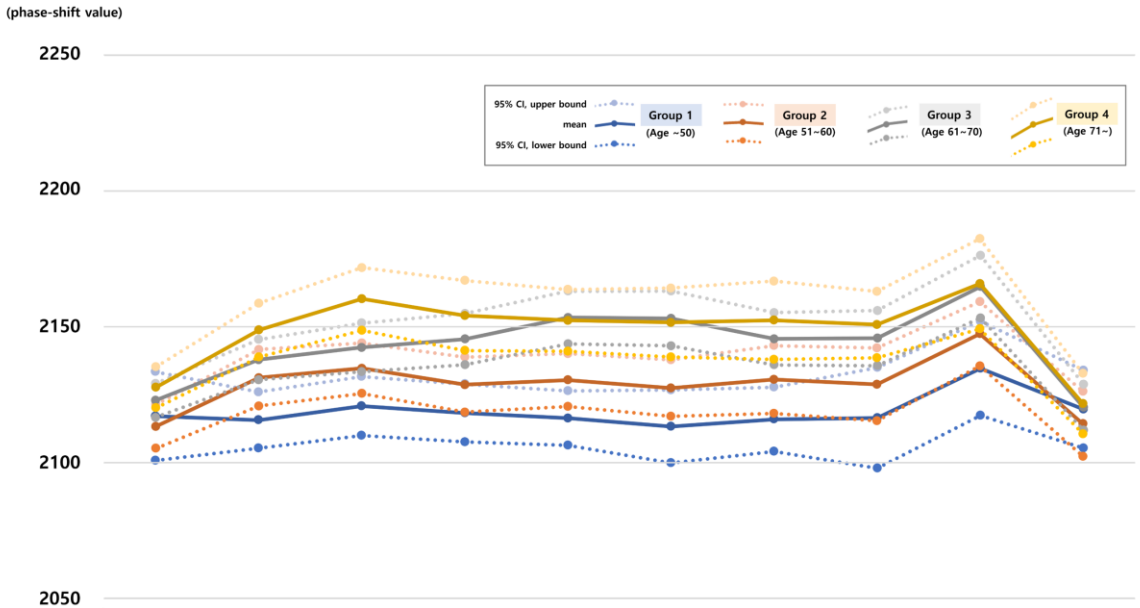

	Seg 01	Seg 02	Seg 03	Seg 04	Seg 05	Seg 06	Seg 07	Seg 08	Seg 09	Seg 10
Between Groups	0.085	0.002**	<0.001***	<0.001***	<0.001***	<0.001***	<0.001***	0.006**	0.03*	0.788
Group 1 vs Group 2	NA	0.303	0.506	0.612	0.230	0.434	0.407	0.731	0.778	NA
Group 1 vs Group 3	NA	0.04*	0.096	0.001**	<0.001***	<0.001***	0.001**	0.044*	0.077	NA
Group 1 vs Group 4	NA	0.001**	0.001**	<0.001***	<0.001***	0.001**	0.001**	0.022*	0.092	NA
Group 2 vs Group 3	NA	0.699	0.676	0.096	0.006**	0.003**	0.302	0.163	0.234	NA
Group 2 vs Group 4	NA	0.056	0.006**	0.014*	0.024*	0.023*	0.132	0.082	0.282	NA
Group 3 vs Group 4	NA	0.274	0.043*	0.856	1.000	1.000	0.965	0.926	0.999	NA

Group 1: age 50 and under, Group 2: age 51 to 60, Group 3: age 61 to 70, Group 4: age 71 and over
Seg: segment, NA: not applicable, *p<0.05, **p<0.01, ***p<0.001

3.3.3. Age and the initial segment signal for normalization

From the groupwide comparison, it was found that there was an age-dependent iron deposition pattern in each segment. However, there are still wide variations that could not be explained by age. We got a hint from the Scatterplot (Figure 3), which has a stable initial part regardless of the group. Furthermore, the initial part seemed to lead the other parts' signals similarly in most individuals in the PD and NC groups. In addition, Segment 1 was less affected by age (Figure 6). Thus, we postulated that the initial segment could represent an individual's iron background.

We performed a linear correlation analysis between age and all segments in the non-MSA-p group (Figure 7). Age and Segment 1 were significantly related to all the other segments. Although age had a correlation with the PSV of Segment 1, its r-value (coefficient of correlation) was very small (r=0.190) compared to the other comparisons.

Figure 7. Linear correlation analysis between age and all segments

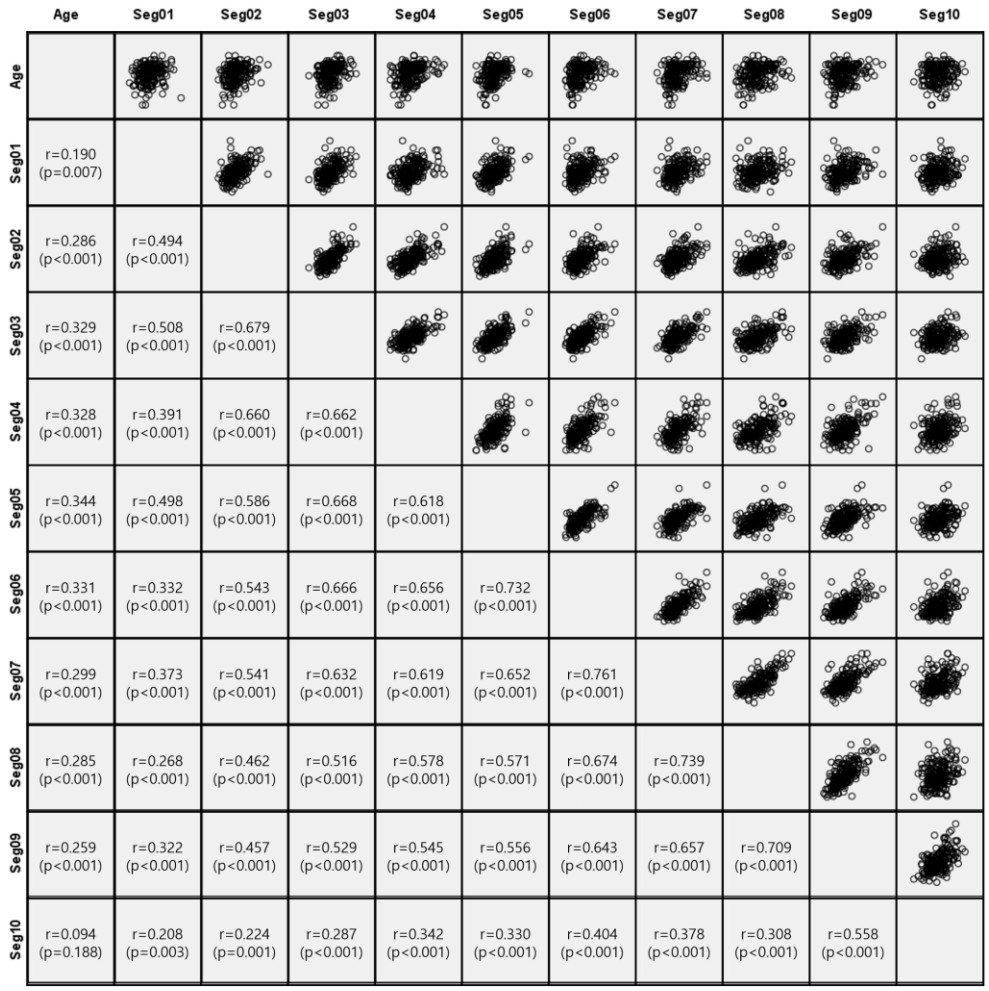

Seg: segment, r: coefficient of correlation

A multiple regression analysis was performed to assess how much age and Segment 1's PSV contribute to each segment's PSV and to estimate the normalized PSV of each segment in MSA-p patients under the assumption of non-MSA-p subjects. Figure 8 shows that the PSV of Segment 1 contributed more to the PSVs of each segment than age did, except for Segment 8.

Figure 8. Standardized coefficients of Segment 1' s phase-shift value and age in multiple regression analyses

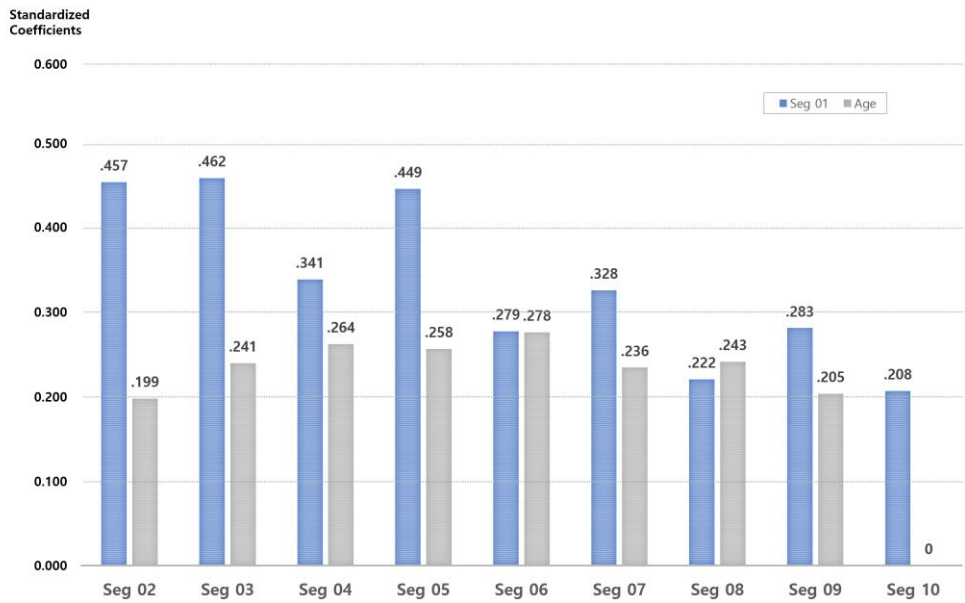

Seg: segment

3.3.4. Differential diagnosis of MSA-p using regression equations

To calculate the PSV difference between MSA-p patients and their assumed normal status, we developed the regression equations for Segment 2 and Segment 9 based on the multiple regression analysis (Table 3). The equation for Segment 10 was not calculated because of the poor predictive power of the regression model.

Table 3. Estimated phase-shift value of each segment assuming normal

Estimated PSV in	Equation
Seg 02	= 931.188 + 0.546*PSV_{Seg01} + 0.746*Age
Seg 03	= 756.082 + 0.623*PSV_{Seg01} + 1.020*Age
Seg 04	= 1022.105 + 0.492*PSV_{Seg01} + 1.193*Age
Seg 05	= 718.353 + 0.638*PSV_{Seg01} + 1.151*Age
Seg 06	= 1154.32 + 0.426*PSV_{Seg01} + 1.331*Age
Seg 07	= 981.595 + 0.512*PSV_{Seg01} + 1.157*Age
Seg 08	= 1314.948 + 0.353*PSV_{Seg01} + 1.213*Age
Seg 09	= 1026.340 + 0.500*PSV_{Seg01} + 1.134*Age

PSV: phase-shift value, Seg: segment, PSV_{Seg01}: PSV of Segment 1

The newly-defined representative values were obtained in various ways (Figure 9). Estimated PSVs, calculated from the regression equations, and original PSVs were used to determine the representative values. The PD and NC groups showed similar patterns between original PSVs and estimated PSVs, but the MSA-p group did not.

Figure 9. Example of defining various representative phase-shift values

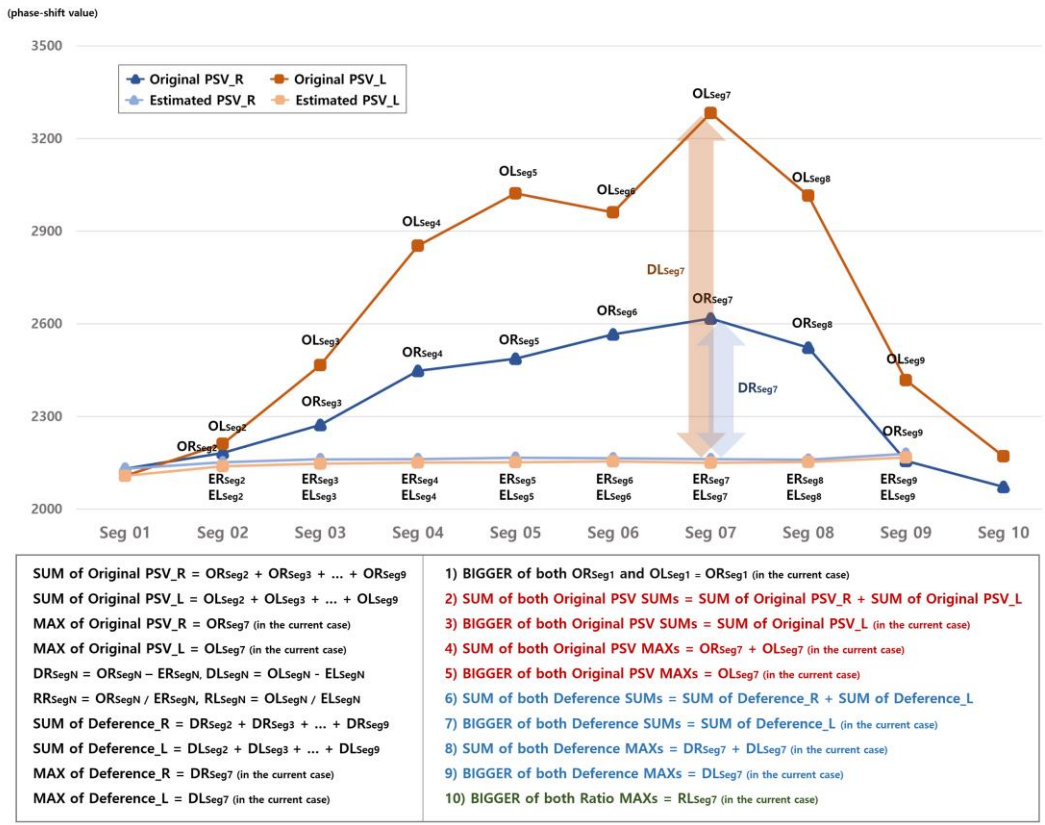

PSV: phase-shift value, Seg: segment, _R: on the right side, _L: on the left side, OL_{SegN}: original PSV of the left side in Segment N, OR_{SegN}: original PSV of the right side in Segment N, ER_{SegN}: estimated PSV of the right side in Segment N, EL_{SegN}: estimated PSV of the left side in Segment N, DL_{SegN}: original PSV minus estimated PSV of the left side in Segment N, DR_{SegN}: original PSV minus estimated PSV of the right side in Segment N, RL_{SegN}: original PSV divided by estimated PSV of the left side in Segment N, RR_{SegN}: original PSV divided by estimated PSV of the right side in Segment N

Figure 10 shows the diagnostic performance with the areas under the curve (AUCs) by the newly-defined representative values. All the results except for the bigger PSV in Segment 1 were statistically significant ($p < 0.001$). In the comparison of the MSA-p and PD groups, 0.872 (65.4% sensitivity and 98.3% specificity) was the highest value in condition 9 which selects a bigger one among the two maximum differences between the original and estimated PSVs of both sides. In comparing the MSA-p and NC groups, the AUC was also similar (0.873 AUC, 69.2% sensitivity, and 97.4% specificity in condition 9). However, the comparisons with condition 10, which indicate a maximum ratio of the original and estimated PSVs, were not so good (0.826 AUCs in common).

The diagnostic yield improved when using the features from a single specified segment rather than whole segments. In Figure 10, conditions 3 and 4 are better than condition 2, and condition 5 is better than condition 4. In addition, with adopting estimated PSVs, the performance seemed to improve. Conditions 6~9 tended to show better performance than conditions 2~5.

Figure 10. Areas under the curve by the newly-defined representative values

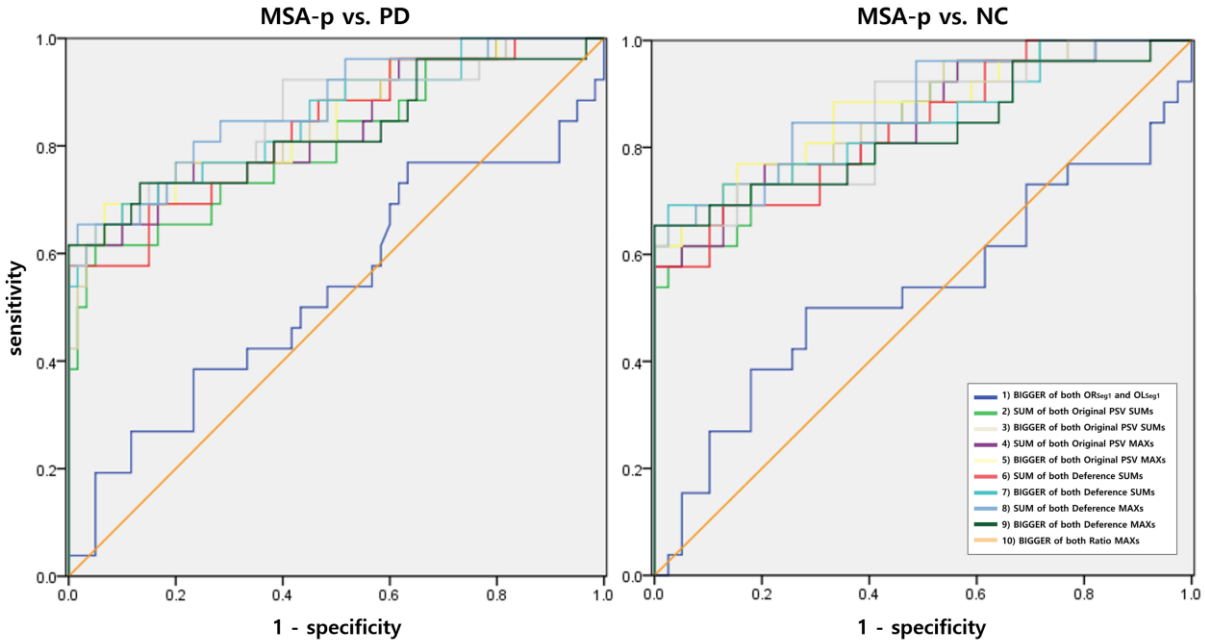

		Only original PSVs				With estimated PSVs				
	1)	2)	3)	4)	5)	6)	7)	8)	9)	10)
MSA-p vs. PD	0.533	0.807	0.844	0.836	0.849	0.833	0.852	0.854	0.872*	0.826
MSA-p vs. NC	0.533	0.850	0.860	0.849	0.871	0.838	0.851	0.852	0.873*	0.826

MSA-p: multiple system atrophy with predominant parkinsonism, PD: Parkinson's disease, NC: normal control, PSV: phase-shift value
*The most representative cases in each comparison set

3.4. Continuous curve-based approach for the lateral rim

From the segment-based approach, we realized that a specified analysis with maximum PSV from one side provided better outcomes in the differential diagnosis of MSA-p. In addition, normalization could enhance diagnostic performance. Therefore, we tried to test a new algorithm with more detailed and characteristic data extracted from continuous PSV curves from anterior to posterior parts. The normalization process with the most anterior part of the putaminal lateral rim was also included.

We displayed the PSV distribution of each section cut into 5 pixels by group (Figure 11). The most anterior parts had consistent patterns and similar PSVs ($p=0.517$) regardless of group. This consistency of the anterior parts was expected to be useful in normalizing the individual raw data, as discussed in the segment-based approach section. Therefore, we adopted each individual average PSV of the initial 5 points (AV5) for normalization.

Figure 11. Anterior-to-posterior distribution of the phase-shift values

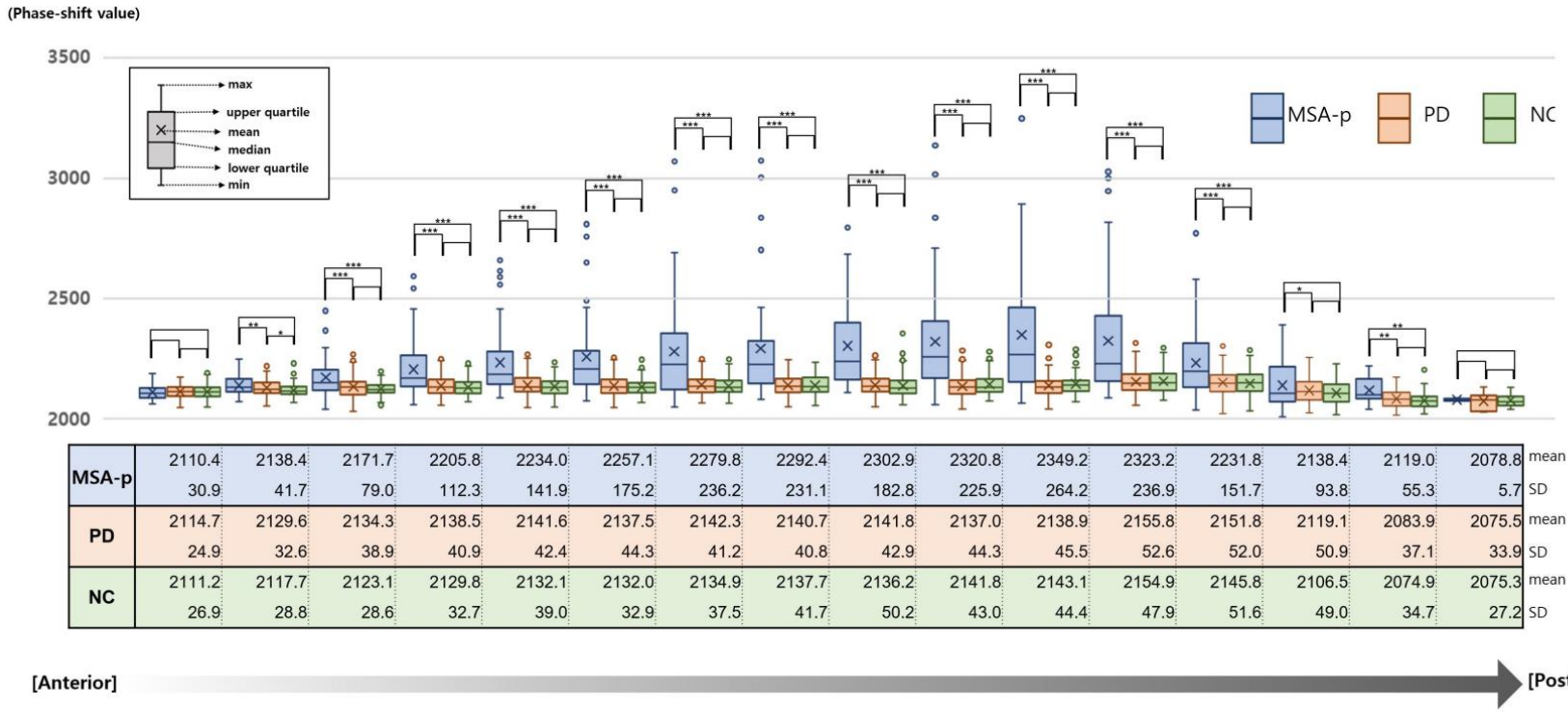

MSA-p	2110.4	2138.4	2171.7	2205.8	2234.0	2257.1	2279.8	2292.4	2302.9	2320.8	2349.2	2323.2	2231.8	2138.4	2119.0	2078.8	mean
	30.9	41.7	79.0	112.3	141.9	175.2	236.2	231.1	182.8	225.9	264.2	236.9	151.7	93.8	55.3	5.7	SD
PD	2114.7	2129.6	2134.3	2138.5	2141.6	2137.5	2142.3	2140.7	2141.8	2137.0	2138.9	2155.8	2151.8	2119.1	2083.9	2075.5	mean
	24.9	32.6	38.9	40.9	42.4	44.3	41.2	40.8	42.9	44.3	45.5	52.6	52.0	50.9	37.1	33.9	SD
NC	2111.2	2117.7	2123.1	2129.8	2132.1	2132.0	2134.9	2137.7	2136.2	2141.8	2143.1	2154.9	2145.8	2106.5	2074.9	2075.3	mean
	26.9	28.8	28.6	32.7	39.0	32.9	37.5	41.7	50.2	43.0	44.4	47.9	51.6	49.0	34.7	27.2	SD

MSA-p: multiple system atrophy with predominant parkinsonism, NC: normal control, PD: Parkinson's disease, SD: standard deviation
*p<0.05, **p<0.01, ***p<0.001
This figure displays the phase-shift values of each section according to the subgroups. Each section was cut into 5 pixels from the anterior to the posterior parts. All the data in this figure were obtained under the condition of '3' height.

3.4.1. Development of the optimal algorithm for differentiating MSA-p

To enhance the diagnostic accuracy of MSA-p, we experimented with the given PSVs under various conditions: 1) by the analyzed side(s) [both sides, one dominant side]; 2) by the "height" number [1, 2, 3, 4]; and 3) by the normalization methods [raw value, raw value-AV5, raw value/AV5]. In each situation, the highest PSV was defined as the representative raw value. The specific representative raw value for each subject was used for the diagnosis of MSA-p versus PD or NC. The values for the AUCs from the ROC curve analysis were calculated for all diagnostic settings (Table 4 and Figure 12). All the results were statistically significant ($p < 0.001$).

Table 4. Areas under the curve according to the diagnostic set

	For both sides				For one dominant side			
	1	2	3	4	1	2	3	4
I. MSA-p vs. PD								
raw value	0.792	0.812	0.811	0.831	0.829	0.838	0.843	0.843
raw value-AV5	0.812	0.817	0.829	0.845	0.834	0.845	0.872*	0.878*
raw value/AV5	0.812	0.817	0.829	0.845	0.841	0.836	0.874*	0.874*
II. MSA-p vs. NC								
raw value	0.818	0.824	0.823	0.837	0.853	0.843	0.847	0.846
raw value-AV5	0.847	0.813	0.836	0.833	0.868	0.834	0.883*	0.854
raw value/AV5	0.844	0.813	0.836	0.835	0.873	0.830	0.883*	0.867

MSA-p: multiple system atrophy with predominant parkinsonism, PD: Parkinson's disease, NC: normal control, AV5: the average of anterior 5 phase shift values

All cases reached statistical significance ($p < 0.001$).

*The representative cases in each comparison set

Figure 12. ROC curves of MSA-p versus PD and MSA-p versus NC

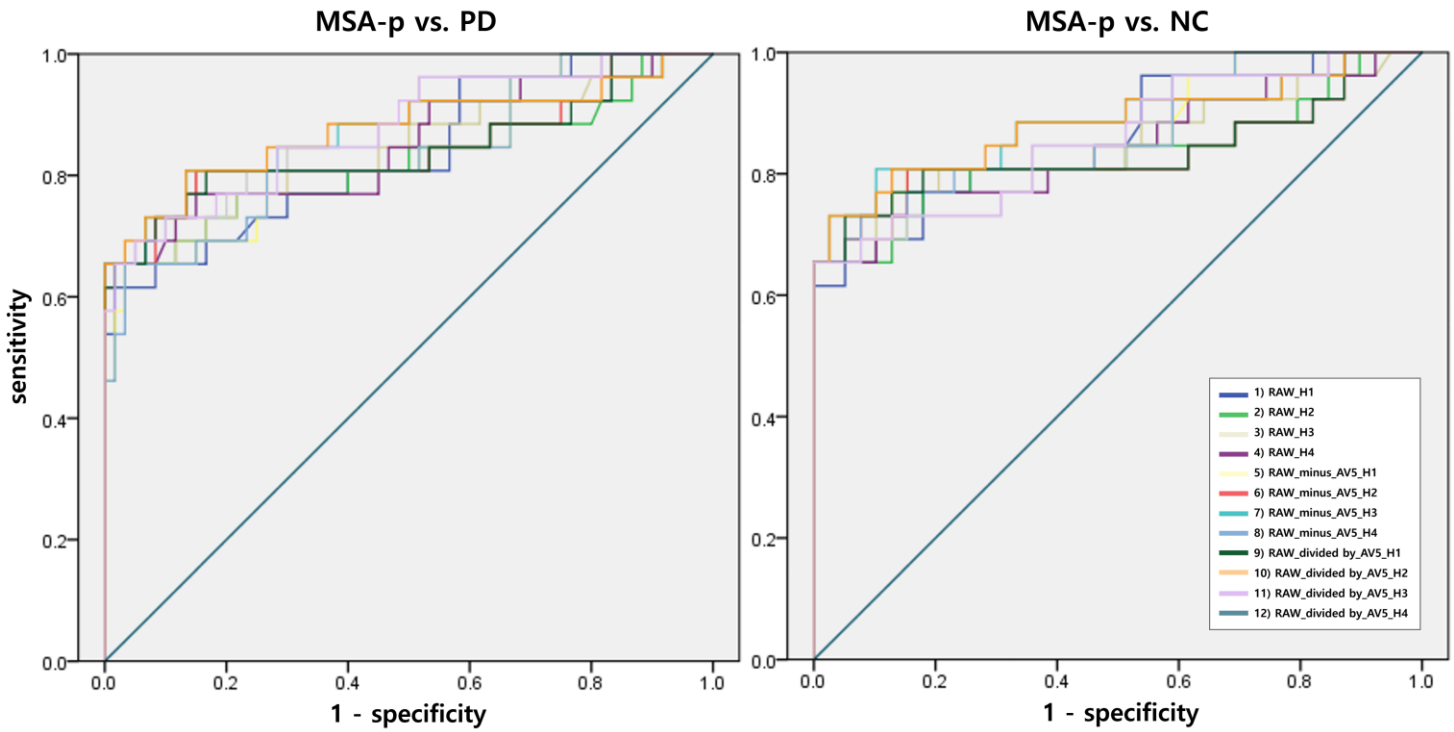

ROC: receiver operating characteristic. MSA-p: multiple system atrophy with predominant parkinsonism, PD: Parkinson's disease, NC: normal control, RAW: raw value, AV5: the average of anterior 5 phase-shift values, H1: height 1, H2: height 2, H3: height 3, H4: height 4

The AUCs tended to be higher with a larger vertical pixel number after normalization with AV-5 and for one dominant side (Table 4 and Figure 12). The AUC for differentiating MSA-p from PD was prominent when the ROC analysis was performed with the representative value obtained from the condition of '3' or '4' vertical pixels, 'raw value-AV5' or 'raw value/AV5', and 'for one dominant side.' In this setting, the means ± standard deviations (SDs) of the representative raw values in the MSA-p and PD groups were 2488.6 ± 356.2 and 2211.5 ± 52.4 ($p<0.001$), respectively.

In the comparison of the MSA-p and NC groups, 0.883 was the highest value in the condition with '3' vertical pixels, 'raw value-AV5' or 'raw value/AV5', and 'for one dominant side.' The means ± SDs of the representative raw values in the MSA-p and NC groups were 2488.6 ± 356.2 and 2205.6 ± 47.3 ($p<0.001$), respectively.

When applying the combination of '3' of height, 'raw value-AV5' or 'raw value/AV5', and 'for one dominant side,' overall sensitivities and specificities were 73.1~80.8% and 86.7~97.4%. More detailed data, including relevant cut-off values, are shown in Table 5.

Table 5. Sensitivity, specificity, and cut-off value in the condition showing the best performance

	raw value-AV5			raw value/AV5		
	sensitivity (%)	specificity (%)	cut-off value	sensitivity (%)	specificity (%)	cut-off value
MSA-p vs. PD	80.8 (73.1)	86.7 (93.3)	156.678 (190.511)	80.8 (73.1)	86.7 (93.3)	1.074 (1.090)
MSA-p vs. NC	73.1 (80.8)	97.4 (89.7)	192.678 (157.367)	73.1 (80.8)	97.4 (87.2)	1.091 (1.072)

AV5: the average of anterior 5 phase shift values, MSA-p: multiple system atrophy with predominant parkinsonism, PD: Parkinson's disease, NC: normal control
This analysis was performed in the condition with '3' of height and 'for one dominant side.'

3.4.2. Subgroup analysis of the MSA-p subjects with a longer disease duration

The number of MSA-p subjects with a disease duration of two or more years was 20. We compared them with the PD subjects according to the dominant side. The highest AUC for differentiating MSA-p from PD was 0.893 when we used the condition of '3' vertical pixels and 'raw value-AV5.' In the case of the MSA-p subjects with a disease duration of three or more years (n=13), the highest AUC was 0.908 under the same conditions.

Chapter 4. Discussion

The early and accurate diagnosis of neurodegenerative disorders is challenging and an important issue in terms of intervening in disease progression. The problem is that early symptoms of MSA-p resemble those of other parkinsonian disorders, and some manifestations arise in the late stage of the disease.[11, 15] Many imaging studies have been performed to overcome the limitations of a symptom-based diagnosis.[13, 26-29] Nevertheless, image-based diagnostics still have limitations resulting from inconsistent manipulation and interpretation. Thus, we introduced a semiautomated algorithm to solve the problem of inconsistency by human raters.

Additionally, in this newly developed algorithm, we focused on the lateral part of the putamen because previous pathological and imaging studies revealed that the most prominent pathological changes in MSA-p start at the posterolateral rim of the putamen.[17, 22, 30] The introduced algorithm worked well for all individuals in the MSA-p group. In other words, the putaminal margins of MSA-p were clear enough to be easily detected by the algorithm. Interestingly, it was not successful in some cases in the PD and NC groups. Their margins were unlikely to be demarcated because of

homogenous and similar signals compared with those in the surrounding regions.

After applying the algorithm, we identified several important features from the scatterplots of PSVs in the putaminal lateral rims. First, the graphs of the PD and NC groups resembled each other. Their variations in the PSVs are relatively narrow from the anterior to posterior parts. This lateral margin analysis would be ineffective in differentiating PD from NC. Second, the MSA-p group showed wide intra- and interindividual variations in the PSVs. In particular, the highest and most diverse PSVs were located on the posterior parts, which is in good agreement with previous reports showing that iron deposition is more predominant in the posterolateral portion of the putamen.[17, 22, 30] Thus, further imaging studies for the differentiation of MSA-p need to focus more on the posterolateral part of the putamen rather than the whole area. Third, the most interesting result from the scatterplot analysis is that the PSVs of the most anterior portion are quite stable in the MSA-p, PD, and NC groups.

In the segment-based approach, we started analysis after designating the average value of each segmented area as a representative value. The first part (Segment 1) showed no statistical difference (Table 2) between the three groups, as shown

in the scatterplot (Figure 3). In particular, there was no statistical difference between PD and NC in all segments. This enabled us to analyze the PD and NC groups together to set up a normalization strategy.

First, we checked whether aging increased iron deposition and whether the change occurred in all the segments. While the first anterior segment seemed to show minor change, most segments showed a pattern of increasing iron deposition with aging. This finding is consistent with the previous studies.[24] The first anterior part had few changes according to age, so it was presumed as a part that has a relatively independent portion from age and reflects individual characteristics. To confirm this, we performed a correlation analysis between age and representative PSVs of all segments. The results showed that the PSV of Segment 1, as well as age, correlated well with the other segments. When multiple regression analysis was performed, the explanatory power by Segment 1 was higher for each than by age.

From the regression equation, the estimated normal value of each segment in MSA-p patients was obtained using their age and the PSV of Segment 1. When we used this normalization method, the best AUCs were 0.872 (MSA-p vs. PD) and 0.873 (MSA-p vs. NC), comparable to previous studies.[21, 22] The advantage of this

analysis is to increase the yield by using normalization with age and the PSV of Segment 1. However, there are also disadvantages. The length of the first segment varies depending on individuals, and the actual representative area could be masked according to segmented points. Given that the iron distribution in MSA-p had considerable variation, the segment-based approach could be good but not enough.

We tried the continuous curve-based approach with the reference value with a fixed length thought to reflect a unique iron background in the putamen regardless of the disorder. AV5 worked well to improve diagnostic accuracy. In the ROC curve analysis, when the normalization method using AV5 was applied, the values of AUCs increased markedly rather than when only 'raw values' were used. There were other factors that were helpful in increasing the AUC values. Several studies reported that many MSA-p patients had asymmetry of parkinsonism with compatible asymmetric putaminal involvement on brain MRI.[7, 12, 22, 31] Therefore, it is presumable that the representative values from one dominant side rather than from both sides could make the differences more distinct. Using 3 or 4 vertical pixels also seemed to enhance accuracy. However, further analysis is required to confirm which

pixel number is the most appropriate or whether larger number has an additional benefit.

The highest values of AUC, sensitivity and specificity in this study were 0.878, 80.8%, and 86.7%, respectively, while those in the previous study were 0.803, 77.8%, and 76.0.[22] There are several explanations for the improvement. We utilized all points along lateral margins and determined the most characteristic values to maximize the differences. We normalized each raw data point with the initial 5 PSVs of each individual subject. In addition, 24 situations were examined for each comparison, and the most effective setting was selected. If the discrimination failure cases by our algorithm were regarded as 'no MSA-p,' the diagnostic yield could increase even more. In the further analysis for the MSA-p patients with a longer disease duration, the AUC values increased up to 0.893 (for the cases of disease duration ≥ two years) and 0.908 (for the cases of disease duration ≥ three years).

As commented in the introduction, the MSA diagnostic criteria were recently revised, and it needs at least one MRI marker to diagnose a "clinically established MSA."[5] Interestingly, there were new imaging criteria for diffusion brain MRI. If a diffusivity of the putamen or middle cerebellar peduncle increases, it is thought to be a supportive MRI marker for "clinically established MSA."

However, there was a difference between structural brain MRI in the operationalized definition. The judgment from diffusion brain MRI should be based on 'quantitative assessments.' Despite the inconvenience of quantification, diffusion brain MRI was accepted as a new imaging diagnostic marker due to its excellent sensitivity and specificity. The recent meta-analysis showed excellent sensitivity and specificity for MSA-p versus PD (90% and 93%, respectively).[29] Of note is that the mean disease duration of MSA-p was higher than in the current study. In this sense, quantitative assessments with iron-sensitive brain MRI could be a future candidate for the clinical diagnosis of MSA.

There are several limitations of this study. First, this study is not based on definite MSA. There could be MSA-p-mimicking conditions, such as PD with early prominent autonomic dysfunction and levodopa responsiveness. Because it is difficult to perform a study with only definite MSA in practice, this is an unavoidable issue in clinical studies. However, we followed the patients more from the time of the workup, and the proportion of probable MSA-p at the final visit was high (20 of 26, 76.9%). Second, data were collected retrospectively from medical records. The data on clinical severity were not included. Additionally, there could be selection bias. Third, there was a discrepancy between the MSA-p and PD

groups in the follow-up period and the duration between the onset and the brain MRI visit. It is widely known that MSA-p progresses more rapidly than PD.[6-8] We included more follow-up clinical data even after the acquisition of brain MRI to render the diagnoses more reliable. Additionally, the ages at the workup were not different between the groups. This means that the confounding effects associated with the age factor, which is well correlated with iron accumulation in the putamen, may be negligible.[24] Fourth, there was no direct comparison with visual assessment, and we collected the SWI data generated by one particular type of MRI machine. Additional investigations are required to prove the new algorithm's superiority and apply it to other iron-specific imaging modalities, especially to QSM, which could reflect iron concentration more precisely. Finally, the current algorithm works semiautomatically. The current algorithm still requires users' help in several steps to prevent detection errors, as shown in Figure 1. It could not be excluded that these manual processes may affect the outcomes of the algorithm. Automating the algorithm to function without the user's intervention and improving all processes from image selection to final diagnosis are currently in progress.

Chapter 5. Conclusion

The semiautomated algorithm using the SWI data is helpful in overcoming rater-related problems and enhancing the diagnostic accuracy of MSA-p from PD. Additionally, we suggested a new personalized approach to reflect the individual iron background and the most effective combinations of several conditions to increase the diagnostic yield. If these additional features, including changes in pons, middle cerebellar peduncle, cerebellum, could be reflected in the advanced algorithm, the diagnostic yield would be better.[21, 32] Further studies are necessary beyond the current limitations with the rapid progression of imaging techniques and artificial intelligence.

Bibliography

1. Gilman S, Low PA, Quinn N, Albanese A, Ben-Shlomo Y, Fowler CJ, et al. Consensus statement on the diagnosis of multiple system atrophy. J Neurol Sci 1999;163:94-98.

2. Gilman S, Wenning GK, Low PA, Brooks DJ, Mathias CJ, Trojanowski JQ, et al. Second consensus statement on the diagnosis of multiple system atrophy. Neurology 2008;71:670-676.

3. Jellinger KA. Neuropathology of multiple system atrophy: New thoughts about pathogenesis. Mov Disord 2014;29:1720-1741.

4. Wenning GK, Tison F, Ben Shlomo Y, Daniel SE, Quinn NP. Multiple system atrophy: a review of 203 pathologically proven cases. Mov Disord 1997;12:133-147.

5. Wenning GK, Stankovic I, Vignatelli L, Fanciulli A, Calandra-Buonaura G, Seppi K, et al. The Movement Disorder Society Criteria for the Diagnosis of Multiple System Atrophy. Mov Disord 2022.

6. Wenning GK, Ben Shlomo Y, Magalhaes M, Daniel SE, Quinn NP. Clinical features and natural history of multiple system atrophy. An analysis of 100 cases. Brain 1994;117 (Pt 4):835-845.

7. Low PA, Reich SG, Jankovic J, Shults CW, Stern MB, Novak P, et al. Natural history of multiple system atrophy in the USA: a prospective cohort study. Lancet Neurol 2015;14:710-719.

8. Wenning GK, Geser F, Krismer F, Seppi K, Duerr S, Boesch S, et al. The natural history of multiple system atrophy: a prospective European cohort study. Lancet Neurol 2013;12:264-274.

9. Quinn NP. How to diagnose multiple system atrophy. Mov Disord 2005;20 Suppl 12:S5-S10.

10. Albanese A, Colosimo C, Bentivoglio AR, Fenici R, Melillo G, Colosimo C, et al. Multiple system atrophy presenting as parkinsonism: clinical features and diagnostic criteria. J Neurol Neurosurg Psychiatry 1995;59:144-151.

11. Osaki Y, Ben-Shlomo Y, Lees AJ, Wenning GK, Quinn NP. A validation exercise on the new consensus criteria for multiple system atrophy. Mov Disord 2009;24:2272-2276.

12. Koga S, Aoki N, Uitti RJ, van Gerpen JA, Cheshire WP, Josephs KA, et al. When DLB, PD, and PSP masquerade as MSA: an autopsy study of 134 patients. Neurology 2015;85:404-412.

13. Bhattacharya K, Saadia D, Eisenkraft B, Yahr M, Olanow W, Drayer B, et al. Brain magnetic resonance imaging in multiple-system atrophy and Parkinson disease: a diagnostic algorithm. Arch Neurol 2002;59:835-842.

14. Brooks DJ, Seppi K, Neuroimaging Working Group on MSA. Proposed neuroimaging criteria for the diagnosis of multiple system atrophy. Mov Disord 2009;24:949-964.

15. Stankovic I, Quinn N, Vignatelli L, Antonini A, Berg D, Coon E, et al. A critique of the second consensus criteria for multiple system atrophy. Mov Disord 2019;34:975-984.

16. Kaindlstorfer C, Jellinger KA, Eschlböck S, Stefanova N, Weiss G, Wenning GK. The Relevance of Iron in the Pathogenesis of Multiple System Atrophy: A Viewpoint. J Alzheimers Dis 2018;61:1253-1273.

17. Matsusue E, Fujii S, Kanasaki Y, Sugihara S, Miyata H, Ohama E, et al. Putaminal lesion in multiple system atrophy: postmortem MR-pathological correlations. Neuroradiology 2008;50:559-567.

18. Lee MJ, Kim TH, Kim SJ, Mun CW, Shin JH, Lee GH, et al. Speculating the timing of iron deposition in the putamen in multiple system atrophy. Parkinsonism Relat Disord 2019;63:106-110.

19. Liu C, Li W, Tong KA, Yeom KW, Kuzminski S. Susceptibility-weighted imaging and quantitative susceptibility mapping in the brain. J Magn Reson Imaging 2015;42:23-41.

20. Hopp K, Popescu BF, McCrea RP, Harder SL, Robinson CA, Haacke ME, et al. Brain iron detected by SWI high pass filtered phase calibrated with synchrotron X-ray fluorescence. J Magn Reson Imaging 2010;31:1346-1354.

21. Lee JY, Yun JY, Shin CW, Kim HJ, Jeon BS. Putaminal abnormality on 3-T magnetic resonance imaging in early parkinsonism-predominant multiple system atrophy. J Neurol 2010;257:2065-2070.

22. Hwang I, Sohn CH, Kang KM, Jeon BS, Kim HJ, Choi SH, et al. Differentiation of Parkinsonism-Predominant Multiple System Atrophy from Idiopathic Parkinson Disease Using 3T Susceptibility-Weighted MR Imaging, Focusing on Putaminal

Change and Lesion Asymmetry. AJNR Am J Neuroradiol 2015;36:2227-2234.

23. Lee JH, Lee MS. Brain Iron Accumulation in Atypical Parkinsonian Syndromes: in vivo MRI Evidences for Distinctive Patterns. Front Neurol 2019;10:74.

24. Li W, Wu B, Batrachenko A, Bancroft-Wu V, Morey RA, Shashi V, et al. Differential developmental trajectories of magnetic susceptibility in human brain gray and white matter over the lifespan. Hum Brain Mapp 2014;35:2698-2713.

25. Gelb DJ, Oliver E, Gilman S. Diagnostic criteria for Parkinson disease. Arch Neurol 1999;56:33-39.

26. Massey LA, Micallef C, Paviour DC, O'Sullivan SS, Ling H, Williams DR, et al. Conventional magnetic resonance imaging in confirmed progressive supranuclear palsy and multiple system atrophy. Mov Disord 2012;27:1754-1762.

27. Meyer PT, Frings L, Rucker G, Hellwig S. (18)F-FDG PET in Parkinsonism: Differential Diagnosis and Evaluation of Cognitive Impairment. J Nucl Med 2017;58:1888-1898.

28. Orimo S, Suzuki M, Inaba A, Mizusawa H. 123I-MIBG myocardial scintigraphy for differentiating Parkinson's disease from other neurodegenerative parkinsonism: a systematic review and meta-analysis. Parkinsonism Relat Disord 2012;18:494-500.

29. Bajaj S, Krismer F, Palma JA, Wenning GK, Kaufmann H, Poewe W, et al. Diffusion-weighted MRI distinguishes Parkinson disease from the parkinsonian variant of multiple system atrophy: A systematic review and meta-analysis. PLoS One 2017;12:e0189897.

30. Han YH, Lee JH, Kang BM, Mun CW, Baik SK, Shin YI, et al. Topographical differences of brain iron deposition between progressive supranuclear palsy and parkinsonian variant multiple system atrophy. J Neurol Sci 2013;325:29-35.

31. Batla A, Stamelou M, Mensikova K, Kaiserova M, Tuckova L, Kanovsky P, et al. Markedly asymmetric presentation in multiple system atrophy. Parkinsonism Relat Disord 2013;19:901-905.

32. Scherfler C, Gobel G, Muller C, Nocker M, Wenning GK, Schocke M, et al. Diagnostic potential of automated subcortical volume segmentation in atypical parkinsonism. Neurology 2016;86:1242-1249.

국문초록

3T 자화강조영상의 조가비핵 가장자리 감지를 위한 알고리즘 개발 및 파킨슨형다계통위축증의 감별진단을 위한 정량적 접근

서울대학교 대학원
의학과 중개의학 전공
이 웅 우

배경 및 목적: 조가비핵의 철분 침착은 파킨슨형 다계통위축증을 파킨슨병과 구별하는데 도움이 되는 중요한 특징이다. 대부분의 기존 연구들은 뇌자기공명영상을 육안으로 판단하거나 조작을 통한 정량적 비교방법을 통해 두 질환을 감별하려고 하였다. 나이, 위치, 개인 특성에 따른 기본적인 철분 분포의 차이를 반영하지 않았다. 조기진단 역시 영상기반 진단에 중요한 목표이다. 우리는 기존 연구들의 불일치 문제와 표준화 문제를 극복하고 진단 성능을 향상시키기 위해 초기 파킨슨형 다계통위축증에 대해 3T 자화강조영상을 사용하는 새로운 반자동 진단 알고리즘을 개발하고 그 진단적 효용성을 연구하였다.

방법: 본 연구에는 파킨슨형 다계통위축증 26 명, 파킨슨병 68 명, 정상대조군 41 명이 포함되었다. 알고리즘은 두단계로 이루어졌다. 1 단계는 가장 뚜렷한 조가비핵 가장자리를 가지고 있는 사진을 골라내는 것이고, 2 단계는 선택된 사진으로부터 철의 농도를 반영하는 phase-shift

value(PSV)를 가장자리를 따라 계산하는 것이다. 세그먼트 기반 접근 방식과 연속 곡선 기반 접근 방식의 두 가지 접근 방식으로 분석을 진행하였다. 세그먼트 기반 접근 방식에서는 전체 조가비핵 측면 테두리를 10 개의 하위 부분으로 나누고 각 부분의 평균값을 사용하였다. 연속 곡선 기반 접근 방식은 각 대상자의 모든 조가비핵의 PSV 를 활용하였다. 다음 단계로 여러 조합 중에서 최상의 감별진단 성능을 보이는 조건을 식별하였다. 각 대상자의 다양한 대표 PSV 를 설정하여 가장 좋은 진단성능을 보이는 조건을 조사하였다.

결과: 고안된 알고리즘은 모든 파킨슨형 다계통위축증 환자의 조가비핵 가장자리를 잘 구분해낸 반면, 8 명의 파킨슨병 및 2 명의 정상대조군의 것은 구별하지 못하였다. 산점도를 통해 각 그룹별 연구 대상자들의 PSV 분포를 확인하였다. 파킨슨형 다계통위축증에서 가장 뚜렷한 전후방 기울기를 보여준 반면, 맨 앞쪽 부분은 그룹에 관계없이 일관된 패턴과 유사한 PSV 를 보였다 ($p=0.517$). 세그먼트 기반 접근법에서 연령은 세그먼트 10 을 제외한 모든 세그먼트에서 PSV 와 상관관계가 있었다. 세그먼트 1 PSV 는 모든 세그먼트에서 연령보다 더 나은 선형 상관관계를 보였다. 연령과 세그먼트 1 의 PSV 에 대한 회귀 방정식은 정규화된 PSV 를 추정하는 데 사용되었다. 수신기 조작 특성 곡선(receiver operating characteristic curve, ROC curve)을 그렸을 때, 파킨슨형 다계통위축증과 파킨슨병을 감별하기 위한 가장 높은 곡선하면적 값은 0.872 였다. 연속 곡선 기반 접근 방식에서는 맨 앞쪽 5 개의 전방점의

평균 PSV 를 표준화에 사용했다. 파킨슨형 다계통위축증과 파킨슨병 사이를 구별할 때는, 3 개 또는 4 개의 수직 픽셀과 표준화 방법, 그리고 양쪽 중 두드러진 한쪽의 값을 활용할 때 수신자 조작 특성 곡선에서 가장 좋은 성능을 보였다. (민감도 80.8%, 특이도 86.7%) 파킨슨형 다계통위축증과 정상대조군을 비교한 결과에서도 민감도 80.8%, 특이도 89.7%로 두 군을 잘 구별하였다. 유병기간이 더 긴 파킨슨형 다계통위축증 환자에 대한 하위 분석은 더 나은 성능을 보여주었다.

결론: 본 반자동화 알고리즘은 조가비핵의 가장자리를 잘 발견하였고, 이를 통해 해당 위치의 철분 분포에 대한 이해를 높일 수 있었다. 각 개인의 철분 상황을 반영하는 새로운 맞춤형 표준화 방법은 파킨슨형 다계통위축증을 파킨슨병 및 정상대조군과 구별해 내는데 도움이 되었다.

주요어: 자화강조영상, 반자동화, 다계통위축증, 파킨슨병, 조가비핵

학 번: 2013-31163